J. Fluid Mech. (1974), *vol.* 63, *part* 3, *pp.* 563–576
Printed in Great Britain

Onset of cellular convection in a salinity gradient due to a lateral temperature gradient

By C. F. CHEN

Department of Mechanical, Industrial and Aerospace Engineering,
Rutgers University, New Brunswick, New Jersey 08903

(Received 18 October 1972 and in revised form 19 November 1973)

We consider the two-dimensional problem of a linearly stratified salt solution contained between two infinite vertical plates. The fluid and the plates are initially at the same temperature. At $t = 0$, one of the plates is given a step increase in temperature, while the other is maintained at the initial temperature. A time-dependent basic flow is thus generated. The stability of such a time-dependent flow is analysed using an initial value problem approach to the linear stability equations. The method consists of initially distributing small random disturbances of given vertical wavelength throughout the fluid. The disturbances may be in the vorticity, temperature or salinity. The linearized field equations are integrated numerically. The growth or decay of the kinetic energy of the perturbation delineates unstable and stable states. Results have been obtained for a wide range of gap widths. The critical wavelength and the critical Rayleigh number compare favourably with those obtained previously in both physical and numerical experiments.

1. Introduction

If a tank of fluid whose density is stratified owing to a salinity gradient is subjected to heating from a side wall, horizontal cellular motion results when the temperature difference exceeds a certain minimum. These cells may be generated by the restraining effects of the top and bottom walls, or they may be a secondary flow pattern generated as a result of a double-diffusive instability. The former process was investigated 40 years ago (Mendenhall & Mason 1932); the diffusive instability effect has been under study only recently (Thorpe, Hutt & Soulsby 1969; Chen, Briggs & Wirtz 1971, hereafter referred to as THS and I respectively). In THS the temperature gradient was established very slowly so that the density deficit due to heating was nearly compensated by the lateral salinity gradient. Because of the rapid diffusion rate of heat as compared with that of salt, a suitably slanted motion of a fluid parcel causes the release of the available potential energy stored in the salt solution. If the motion thus induced can overcome viscous damping, flow instability results. This phenomenon was indeed predicted by THS using a linear stability analysis in which the small vertical velocity field and the non-diffusive wall effects near the two walls were ignored. According to that theory

the critical value of the thermal Rayleigh number Ra is related to the solute Rayleigh number R_S by

$$Ra = 0{\cdot}059(-R_S)^{\frac{5}{6}}, \tag{1}$$

where $Ra = g\alpha\Delta T D^3/\kappa\nu$ and $R_S = g\beta(\partial S/\partial Z)\, D^4/\kappa_S\nu$, in which g is the gravitational acceleration, α and β the coefficients of expansion due to heat and salt, ΔT the temperature difference across the plates, set a distance D apart, κ and κ_S the diffusivities of heat and salt, and ν the kinematic viscosity. In this expression the ratio of diffusivities $\kappa/\kappa_S = 101$. In a recent paper Hart (1971) solved the stability problem with the boundary-layer flow taken into account. He showed that the boundary-layer flow was stabilizing whereas the interior almost quiescent region was destabilizing. The critical condition (1) becomes asymptotically correct for large values of $-R_S$, which is usually the case of interest. The theoretical prediction has been confirmed by experiments performed by THS in 3·6 and 6 mm slots.

Our experiments (described in I) were carried out in a wide tank (12·7 cm across) and the temperature of one side wall was increased quite suddenly (the time constant for this temperature rise to penetrate the wall was about 3 min). The basic state was a time-dependent one. A natural length scale in this situation is the height h through which a heated fluid element must rise in order to become neutrally buoyant in the given density gradient. By carrying out a number of experiments, we have determined that the critical thermal Rayleigh number R based on h above which cellular convection occurs is $15\,000 \pm 2500$. Had the basic state been a steady one arrived at by heating the side wall slowly, (1) would have given a critical Rayleigh number based on h

$$R = 420L^2, \tag{2}$$

where L is the width of the tank normalized with respect to h. In our tests, in which $h \sim 1$ cm, such a critical Rayleigh number would have been ~ 60000. When the heating is applied impulsively, the velocity generated near the walls is quite high initially, thus inducing a large salinity gradient. Coupled with a large temperature gradient near the hot wall, a critical state may be reached even though the temperature difference imposed may be smaller than the critical value obtained for the steady basic state. Our experiments yielded a critical wavelength ranging from $\sim 0{\cdot}7\,h$ to h with no discernible trend with the Rayleigh number.

A more detailed laboratory study of the initial formation of the cells and the structure of the quasi-steady convection layers has been carried out by us more recently (Wirtz, Briggs & Chen 1972, hereafter referred to as II). Also included in that paper are the results of numerical experiments carried out by integrating the nonlinear equations governing the two-dimensional motion of a stratified fluid subjected to sudden heating from a side wall. When the fluid was in a container, our numerical results showed that at large Rayleigh numbers cells were generated successively inward from the top and bottom boundaries in agreement with the observations of Mendenhall & Mason (1932). For an infinite slot, periodic boundary conditions were applied over a vertical distance chosen on the basis of

experimental results. At a Rayleigh number of 10^5 and gap width $L = 1{\cdot}3$, cells were generated when a continuous input of small random disturbances in the vorticity was applied. Detailed mappings of the salt, temperature and velocity fields were obtained. These were essentially *ad hoc* cases; no systematic searching for the fastest-growing wave was attempted, nor were any wide-gap cases calculated because of the prohibitive computer time that would be involved.

In the present work we examine the problem using the linear stability approach to answer the following questions. What is the effect of gap width on the onset of secondary flow, especially at large gaps $L \sim 5$? How does the critical wavelength vary with the Rayleigh number? What is the mechanism of the initial stages of diffusive instabilities?

The method consists of initially distributing small random disturbances in the fluid. The subsequent motion of the fluid is obtained by numerically integrating the linearized equations, assuming a sinusoidally height-dependent perturbation. This involves far less computer time than the previous nonlinear calculations.

The basic state is classified as stable or unstable according to whether the kinetic energy of the perturbations decays or grows with time. The reasons for choosing this criterion are given detailed discussion in Liu & Chen (1973). This method has been used by Foster (1965) and Gresho & Sani (1971) for studying the stability of a fluid layer with time-dependent temperature gradients, and by Chen & Kirchner (1971) and Chen, Liu & Skok (1973) for studying the stability of time-dependent circular Couette flows. In the present study consistent results are obtained whether the initial disturbances are in the vorticity, temperature or salinity.

The wavelength of the initial disturbances is systematically varied; that wave which attains the fastest growth is the critical one. Results have been obtained for $1 \leqslant L \leqslant 8$. The critical wavelength and Rayleigh number thus obtained compare favourably with those previously obtained in physical and numerical experiments reported in I and II.

2. Equations and methods of calculation

Consider the two-dimensional problem of a linearly stratified fluid contained between two infinite vertical plates separated by a distance L'. The density of the fluid may be approximated by

$$\rho' = \rho'_0[1-\alpha(T'-T'_0)+\beta(S'-S'_0)], \tag{3}$$

where

$$\alpha = -\frac{1}{\rho'}\left(\frac{\partial \rho'}{\partial T'}\right)_{p',S'}, \quad \beta = \frac{1}{\rho'}\left(\frac{\partial \rho'}{\partial S'}\right)_{p',T'}, \tag{4}$$

in which T' and S' denote temperature and salinity, respectively, and the subscripts 0 denote reference values. Initially, the fluid is at a uniform temperature T'_0 and the density stratification is due to the salinity gradient alone. At $t = 0$ the temperature of one of the plates is raised to $T'_0 + \Delta T'$ and a convective flow is generated. We investigate the conditions under which the flow will evolve into horizontal cellular motion.

We have demonstrated in I that the natural length scale for the present problem is the height through which a heated element would rise in the given stratified surroundings to become neutrally buoyant:

$$h = \alpha\Delta T'/[-\rho'^{-1}(\partial\rho'/\partial z')]_0 = \alpha\Delta T'/[-\beta(\partial S'/\partial z')]_0.$$

Using h as the basic length and the thermal diffusion time h^2/κ as the basic time unit, the non-dimensional vorticity equation in the Boussinesq approximation is

$$\frac{D\omega}{Dt} = \sigma\nabla^2\omega - \sigma R\left(\frac{\partial T}{\partial x} - \frac{\partial S}{\partial x}\right). \tag{5}$$

σ denotes the Prandtl number and the Rayleigh number R is defined in terms of the length scale h as

$$R = (g\alpha\Delta T'/\nu\kappa)\,h^3, \tag{6}$$

with the gravitational acceleration g in the $-z$ direction. It has been assumed that all fluid properties are constant. The non-dimensional temperature and salinity are defined as

$$T = (T' - T'_0)/\Delta T', \quad S = -(S' - S'_0)/h(dS'/dz')_0. \tag{7}$$

With this definition of S, the initial salinity gradient is -1. The heat and salt diffusion equations are

$$DT/Dt = \nabla^2 T, \tag{8}$$

$$DS/Dt = (\kappa_S/\kappa)\nabla^2 S. \tag{9}$$

The relationship between the vorticity and stream function, and the definition of the stream function are

$$\nabla^2\psi = \omega, \tag{10}$$

$$\partial\psi/\partial z = u, \quad \partial\psi/\partial x = -w. \tag{11}$$

The initial conditions are

$$T(x, z, t < 0) = 0, \quad dS/dz = -1. \tag{12}$$

The boundary conditions are $T(0, z) = 1$,

$$T(L, z) = u(0, z) = u(L, z) = w(0, z) = w(L, z) = 0, \tag{13}$$

$$\partial S/\partial x = 0 \quad \text{at} \quad x = 0, L.$$

The basic convective state admits a solution which consists of purely vertical motion. This motion is initially oscillatory at the buoyancy frequency and approaches a steady state in which the salt distribution is linear across the gap except in the neighbourhood of the walls, and there is slow motion up the heated plate and down the other plate (Hart 1971).

Using the subscripts 0 and 1 to denote the basic and perturbed states respectively, the linearized equations are

$$\frac{D_0\omega_1}{Dt} = \sigma\nabla^2\omega_1 - \sigma R\frac{\partial}{\partial x}(T_1 - S_1) - u_1\frac{\partial\omega_0}{\partial x}, \tag{14}$$

$$\frac{D_0 T_1}{Dt} = \nabla^2 T_1 - u_1\frac{\partial T_0}{\partial x}, \tag{15}$$

$$\frac{D_0 S_1}{Dt} = \frac{\kappa_S}{\kappa}\nabla^2 S_1 - u_1 \frac{\partial S_0}{\partial x} + w_1, \tag{16}$$

$$\nabla^2 \psi_1 = \omega_1; \quad \partial\psi_1/\partial z = 1, \quad \partial\psi_1/\partial x = -w_1, \tag{17}$$

in which

$$\frac{D_0}{Dt} = \frac{\partial}{\partial t} + w_0 \frac{\partial}{\partial z}. \tag{18}$$

The perturbation quantities u_1, w_1 and T_1 all vanish at the boundary and S_1 has zero x-derivative at the two walls. The equations governing the basic flow are quite similar to the above set and need not be written out here.

The results of our physical and numerical experiments indicate that the perturbed state is periodic in z. We therefore assume that the perturbed quantities have the following form:

$$\omega_1 = (\omega_r + i\omega_i)\, e^{iKz}, \quad \text{etc.}, \tag{19}$$

in which the subscripts r and i denote real and imaginary parts, respectively. When these are substituted into (14)–(18) and the real and imaginary parts separated, we obtain a set of eight simultaneous equations. Six of these prescribe the time evolution of T_1, S_1 and ω_1 and two relate the stream function to the vorticity.

The calculation procedure is to assume small random perturbations in the vorticity, temperature or salinity as initial conditions. The time evolution of the motion generated by these initial disturbances is obtained by numerically integrating the above set of equations as well as the basic flow equations. The growth or decay of the kinetic energy of the perturbed flow serves to indicate whether the basic flow is unstable or stable.

The kinetic energy of the perturbation flow per wavelength is

$$E_p = \tfrac{1}{2}\rho_0' \frac{\kappa^2}{h^2} \int_0^{2\pi/K} \int_0^L [1 - \alpha\Delta T'(T+S)]\,(u^2+w^2)\, dx\, dz. \tag{20}$$

Since $\alpha\Delta T'$ is generally of order 10^{-3} for the Rayleigh numbers of interest, the above expression may be rewritten as

$$\tfrac{1}{2}\rho_0' \frac{\kappa^2}{h^2} \int_0^{2\pi/K} \int_0^L (u^2+w^2)\, dx\, dz = \tfrac{1}{2}\rho_0' \frac{\kappa^2}{h^2} \frac{\pi}{K} \int_0^L \left[\kappa^2(\psi_r^2 + \psi_i^2) + \left(\frac{\partial\psi_r}{\partial x}\right)^2 + \left(\frac{\partial\psi_i}{\partial x}\right)^2\right] dx. \tag{21}$$

The kinetic energy of the basic flow is

$$E_B = \tfrac{1}{2}\rho_0' \left(\frac{\kappa^2}{h^2}\right) \frac{\pi}{K} \int_0^L w_0^2\, dx. \tag{22}$$

In the case of initial vorticity perturbations, the kinetic energy of the perturbations is normalized with respect to its initial value. In the case of initial temperature or salinity perturbations, the perturbation kinetic energy is normalized with respect to the initial potential energy. Suppose that the initial salinity perturbation is δS; the increase in potential energy per unit mass is

$$\text{P.E.} = gh\alpha\Delta T' \int_0^{2\pi/\kappa} \int_0^L (\delta S)^2\, dx\, dz. \tag{23}$$

The ratio of the kinetic energy of the perturbations to the initial potential energy, after some cancellation and re-arrangements, is

$$\frac{1}{2\sigma R}\left[\int_0^{2\pi/K}\int_0^L (u^2+w^2)\,dx\,dz\right]\Big/\left[\int_0^{2\pi/K}\int_0^L (\delta S)^2\,dx\,dz\right]. \tag{24}$$

For initial temperature perturbations, δS is replaced by δT.

The calculations are initiated by assigning small random perturbations in vorticity, temperature or salinity at all grid points. The values of the random perturbations in vorticity lie between 0 and 10^{-4}, whereas those for temperature or salinity perturbations lie between 0 and 10^{-8}. These different ranges of values are chosen so that the initial kinetic energy in the case of vorticity perturbations and the initial potential energy in the case of temperature or salinity perturbations are of the same order of magnitude: $\sim 10^{-10}$. The evolution of the motion generated by the side-wall heating as well as the perturbations is monitored by numerical integration of the basic and perturbation equations for a particular value of the wavenumber K. The time-dependent diffusion equations are written in finite-difference form, using forward time differences and central space differences. The integration proceeds forward in time, with an increment Δt which must be small to ensure stability. Of the three diffusion equations, the vorticity equation places the upper limit on the time steps, since $\sigma \sim 6$ and $\kappa_S/\kappa \sim 0{\cdot}01$. In the computations we take

$$\Delta t = 0{\cdot}4(\Delta x)^2/\sigma.$$

The equation relating the vorticity and stream function, when written in finite-difference form, results in a tridiagonal matrix form which can be solved by Gaussian elimination (see, for example, Keller 1968, p. 72). The normalized kinetic energy of the perturbations is evaluated at each time step. The wavenumber K is systematically varied to obtain the fastest-growing wave. The accuracy of this numerical scheme has been tested by us for a steady Couette flow. The critical Taylor number predicted by this method was found to be within 0·5 % of the accepted value.

3. Results and discussion

Our physical experiments (I) were carried out in a tank whose width was very large compared with the characteristic length h. In the numerical experiment (II), in order to bring the number of grid points and the computation time to reasonable magnitudes, the gap was fixed to be of the same order of magnitude as h. In fact, for $R = 10^5$, the gap was $1{\cdot}3h$. For the present calculations, since we are dealing with linear equations L is varied from 1 to 8. The physical constants are the same as those used in II, and they are listed below:

$$\nu = 0{\cdot}93\times10^{-2}\,\mathrm{cm^2\,s^{-1}},\quad \kappa = 1{\cdot}488\times10^{-3}\,\mathrm{cm^2\,s^{-1}},\quad \kappa_S = 0{\cdot}937\times10^{-2}\kappa,$$

$$\alpha = 3{\cdot}06\times10^{-4}\,^\circ\mathrm{C^{-1}},\quad \sigma = 6{\cdot}25.$$

For all calculations, the initial density gradient is set at $-1{\cdot}64\times10^{-3}\,\mathrm{cm^{-1}}$. With this set of values, at $R = 10^5$ the temperature difference ΔT is 5·16 °C and the length scale is 0·96 cm.

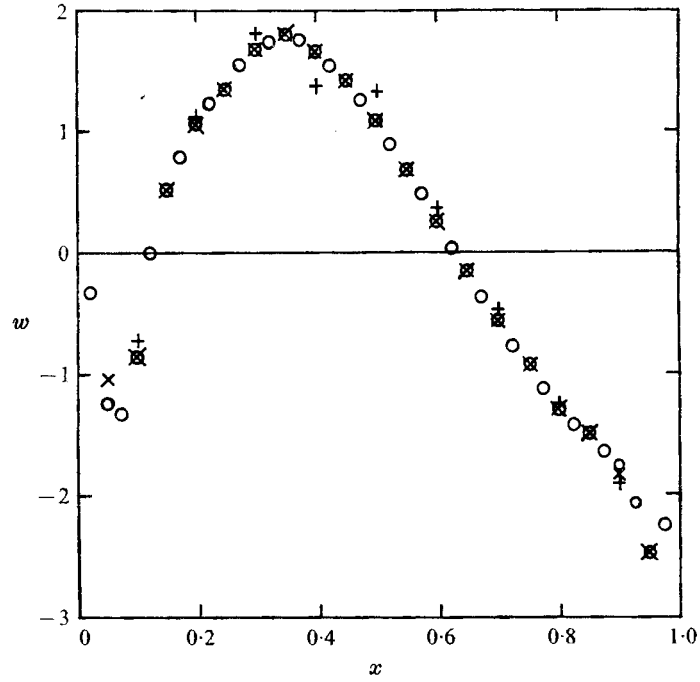

FIGURE 1. Vertical velocity of basic flow at $t = 0{\cdot}06$. +, $\Delta x = 0{\cdot}1$; ×, $\Delta x = 0{\cdot}05$; ○, $\Delta x = 0{\cdot}025$.

The basis for selecting the number of grid points in $0 \leqslant x \leqslant L$ is the accuracy of results, and at the same time economy of computing time. For a test case, calculations are made with $\Delta x = 0{\cdot}1$, $0{\cdot}05$ and $0{\cdot}025$ with $L = 1$ and $R = 10^5$. For the basic temperature distribution $\Delta x = 0{\cdot}1$ suffices. The requirement for the basic velocity distribution is more stringent. As shown in figure 1, Δx needs to be $0{\cdot}05$ or smaller in order to yield accurate results in the main body of the flow. The slight discrepancy near the two walls is not expected to affect the instability results, since it is in these regions that diffusive instability is inhibited. It is to be noted that the actual magnitude of the velocity is extremely small. A value of the non-dimensional velocity of unity corresponds to approximately $1{\cdot}5 \times 10^{-3}$ cm/s.† The growth rate of the perturbation kinetic energy is unreasonably large when $\Delta x = 0{\cdot}1$, as shown by table 1. However, the differences between results with $\Delta x = 0{\cdot}05$ and $0{\cdot}025$ are quite tolerable especially in view of the fact that a consistent value of the critical wavelength is obtained for both cases. The computing time would increase more than four fold if the smaller Δx were used. For all subsequent calculation, Δx is set to be $0{\cdot}05$. This distance is larger than the salt diffusion length up to the time of onset of secondary flow. But the salt transport is almost entirely due to convection except very close to the wall, where the salinity is determined by the non-diffusive wall boundary condition.

† We also note that the ratio of the velocity scale used by Hart to ours is RL^2.

Δx	Growth rate at $E = 10^3$	Time to reach $E = 10^3$
0·1	256	0·060
0·05	92	0·133
0·025	87	0·148

TABLE 1

Development of the basic flow

From Hart's (1971) analysis, it is known that the sideways diffusive instability is initiated in a region where the horizontal gradients of temperature and salinity are nearly the same. Any suitably slanted movement of a parcel of fluid causes the release of available potential energy when the temperature is equilibrated. If the lateral gradients are large enough, the motion caused by the buoyancy difference overcomes viscous damping and secondary flow ensues. The boundary-layer regions near the walls are stabilizing because of the nearly constant salinity distribution forced by the non-diffusive wall.

In the present time-dependent case, the step increase in temperature is imposed on one wall impulsively. An upward flow is immediately generated along the heated wall, thus establishing a horizontal salinity gradient. The onset of diffusive instability will be predicted under the conditions that $T_x - S_x$ is nearly zero and at the same time T_x is large. In figure 2 we have displayed $T_x - S_x$ for $L = 1$ and $R = 10^5$ at $t = 0{\cdot}015$, 0·035, 0·135 and 5. At the earliest time $t = 0{\cdot}015$. the large negative temperature gradient near the hot wall is manifested by the large negative values of $T_x - S_x$. There is also a small region near the other wall where $T_x - S_x$ is negative owing to the positive salinity gradient as a result of downward motion. However, there is a region occupying about one third of the gap width within which $T_x - S_x = 0$. This equal-gradient region expands towards the hot wall as time goes on. At $t = 0{\cdot}135$ the distribution of $T_x - S_x$ is quite close to its asymptotic value represented by $t = 5$ curve. Within the region $x \leqslant 1$ the time evolution of $T_x - S_x$ for larger gap widths is almost identical to the $L = 1$ case except that the equal-gradient region extends beyond $x = 1$.

The temperature gradient at any point decreases from its initial value of 0 to its asymptotic value of $-1/L$. If the point is relatively close to the hot wall, then the temperature gradient will first reach a minimum then increase towards $-1/L$. The evolution of the temperature gradient at $x = 0{\cdot}5$ for $L = 1$ is shown in figure 3. Within the time period $t \leqslant 0{\cdot}2$, the same rise curve for T_x is obtained for all the gap widths considered. In particular, the values for $L = 5$ are shown on the same figure. In fact the temperature distribution for $L = 2$ at $t = 0{\cdot}2$ is almost indistinguishable from that for $L = \infty$. From the results shown in figures 2 and 3, it is seen that diffusive instability will be triggered at approximately the same time for a given supercritical Rayleigh number regardless of gap width so long as $L \geqslant 1$. This fact is borne out in the perturbation calculations.

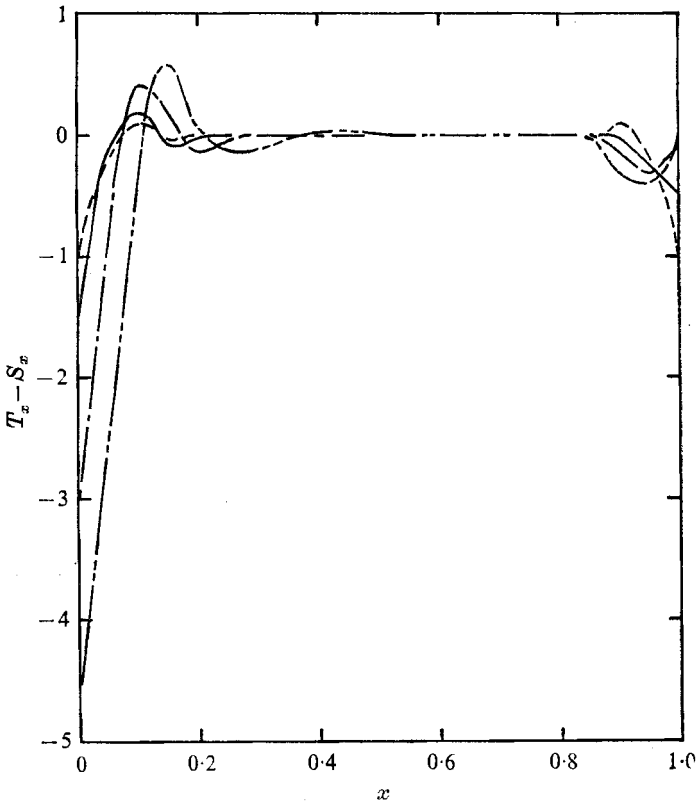

FIGURE 2. Evolution of $T_x - S_x$ for $L = 1$. — · · —, $t = 0{\cdot}015$; — · —, $t = 0{\cdot}035$; ——, $t = 0{\cdot}135$; – – – –, $t = 5{\cdot}0$.

Development of perturbation kinetic energy

Gresho & Sani (1971), in their investigation of the stability of a horizontal fluid layer subjected to a step change in temperature, have found that initial temperature disturbances assume a very much faster growth rate than initial velocity disturbances. In their problem, a temperature disturbance gives rise to unbalanced buoyancy forces immediately, whereas a velocity disturbance can generate such a force only when the temperature of the fluid has been altered by diffusion from the boundary. In the present case, owing to the initial stratification, any disturbance in vorticity, temperature or salinity would immediately produce buoyancy imbalance. It is, therefore expected that the normalized perturbation kinetic energy would behave in a similar manner, whether the initial perturbations are in ω, T or S. This is confirmed by a test case for $L = 1$. The growth rate of the perturbation kinetic energy is essentially the same for all three types of initial perturbations. They all yield the same critical wavelength of $\lambda_c = 0{\cdot}54$. For all subsequent calculations initial vorticity perturbations are used because we think that this type of disturbance is most likely to occur in a laboratory.

A systematic search at $R = 10^5$ for $L = 2$, 3, 4 and 5 yields an identical

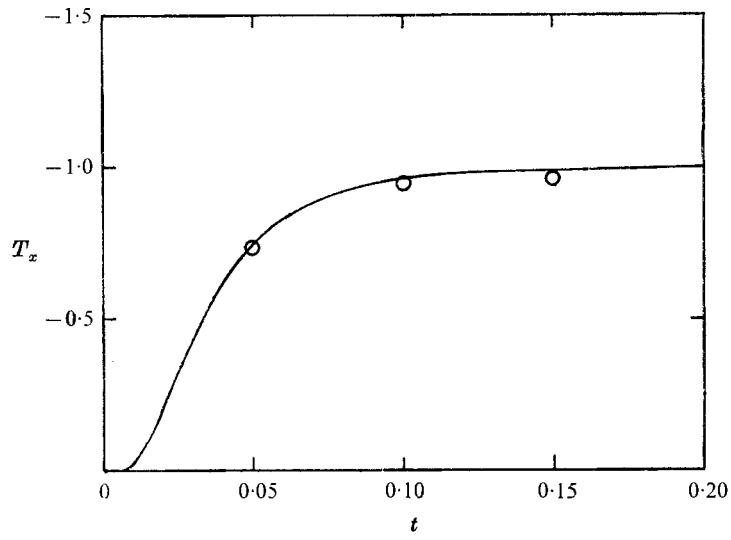

FIGURE 3. Evolution of temperature gradient at $x = 0{\cdot}5$. —, $L = 1$; ○, $L = 5$.

critical wavelength of 0·56, slightly higher than for the narrow-gap case $L = 1$. In the numerical experiments reported in II, for the same Rayleigh number but for $L = 1{\cdot}3$, the size of the cells can be estimated from the streamline plots to be about $0{\cdot}65h$. The results of physical experiments (I; II), obtained in a wide tank, show that the cell sizes ranged from $0{\cdot}67h$ to $0{\cdot}97h$. The difference between the present results and the results of numerical simulation is due to the selection of the vertical extent of the region to be calculated in II. Once the region has been selected, because of the periodic conditions imposed on the boundaries, an integral number of cells will result, and the size of the cells certainly will be biased. In our physical experiments reported both in I and II, we have observed that there was a continuous merging process of the cells or rolls soon after the onset of cellular motion. The present calculation obtains a critical wavelength which determines the initial size of the boundary motion. As the amplitude of the motion becomes finite and merging processes set in, the cell size will increase. The cell sizes in I were obtained by counting the number of cells in the entire test tank at $t = 20$ min. It is then expected that these cells will be larger than those right at the onset of secondary motion.

In figure 4 growth curves of the perturbation kinetic energy for all cases considered at $R = 10^5$ are shown. The normalized perturbation kinetic energy decreases sharply at first owing to viscous damping, then grows exponentially. The growth rates of all these curves are quite similar, and the time for E to attain 10^3 ranges from 0·135 to 0·155 or approximately 100 s in real time. It is interesting to note that, in the calculations of II, the total kinetic energy of the system starts to depart from the kinetic energy of the basic flow at about 100 s (see II, figure 13). The streamline plots and temperature contour maps (II, figures 9 and 10) show that cellular structures are discernible at 160 s. In one of the physical experiments carried out by Wirtz (1971, figure 20) for a Rayleigh number of $3{\cdot}7 \times 10^5$,

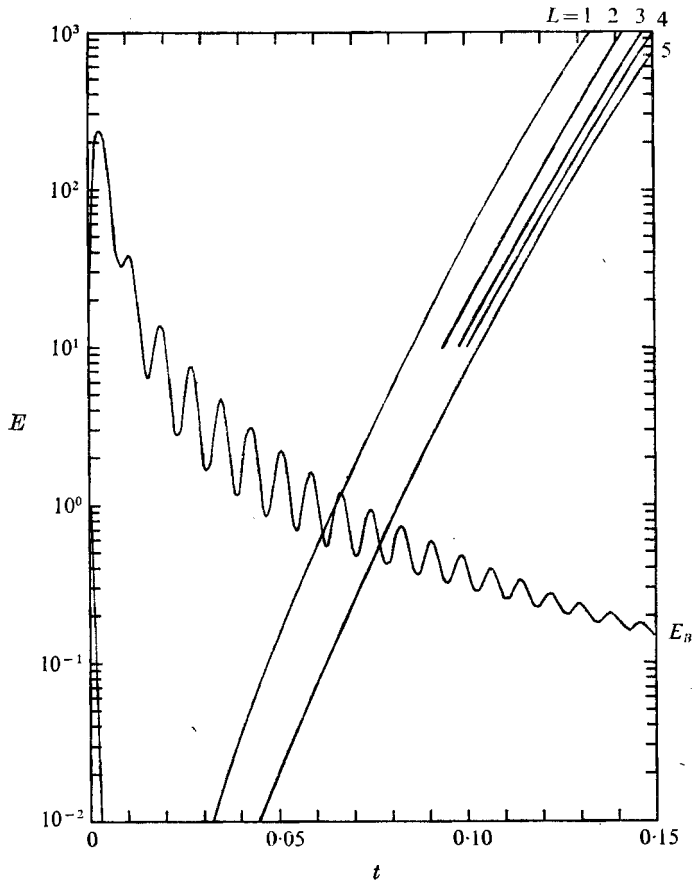

FIGURE 4. Growth of perturbation kinetic energy at $R = 10^5$. $\lambda_c = 0{\cdot}54$ for $L = 1$, $\lambda_c = 0{\cdot}56$ for $2 \leqslant L \leqslant 5$.

the cine-film record of the experiments shows that the onset of cellular motion occurs between 90 and 100 s.

In the same figure, the energy E_B of the basic flow for $L = 2$ is also shown. It oscillates with a decreasing amplitude but with a constant circular frequency of $0{\cdot}2\,\mathrm{s}^{-1}$, which is the Brunt–Väisälä frequency of the salinity gradient used.

A series of calculations made for $L = 5$ at different Rayleigh numbers shows that the critical wavelength decreases slightly as the Rayleigh number is increased. Of course the time needed for E to reach 10^3 decreases as the Rayleigh number is increased. The results are summarized in table 2, in which t_3 denotes the time at which $E = 10^3$.

Transition regime

Our physical experiments were carried out in a wide tank with $L \sim 12$. The steady-state critical Rayleigh number for this width according to (2) is approximately 60000. The experimental results show that with an impulsively applied temperature difference the critical Rayleigh number is 15000 ± 2500. It is reasonable to believe that this critical value will be obtained as long as the width of the

R	λ_c	t_3 Non-dimensional	t_3 Dimensional (s)
$0{\cdot}5 \times 10$	0·63	0·335	145
$1{\cdot}0 \times 10$	0·56	0·155	97
$5{\cdot}0 \times 10$	0·55	0·037	52

TABLE 2

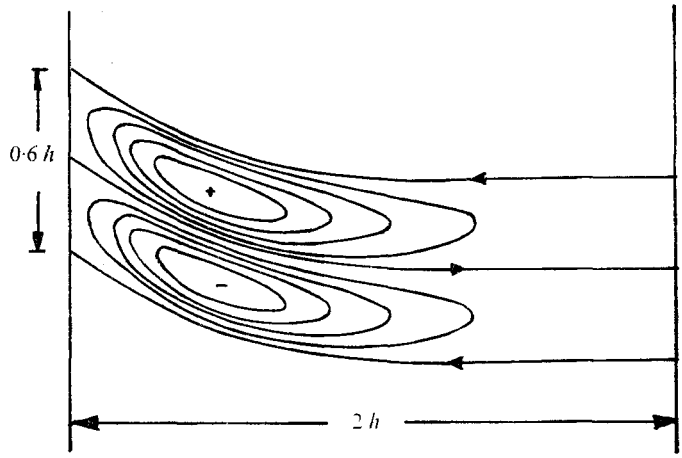

FIGURE 5. Perturbation streamlines at $t = 0{\cdot}15$, $R = 10^5$, $\lambda = 0{\cdot}6$. $\psi/\psi_{\max} = \pm 1, \pm 0{\cdot}8, \pm 0{\cdot}6, \pm 0{\cdot}4, \pm 0{\cdot}2, 0$; $\psi_{\max} = 3{\cdot}9 \times 10^{-5}$.

tank is such that the steady-state critical Rayleigh number exceeds 17500. We have considered a case with $L \approx 8$ for which the steady-state critical Rayleigh number is 26900. Calculations were made for $R = 10^4$ and 2×10^4. For a subcritical Rayleigh number of 10^4, E drops to a very small value initially, then grows to a maximum of $1{\cdot}33 \times 10^{-4}$ at $t = 1{\cdot}44$ (or 28 s) then decays steadily. For a supercritical Rayleigh number of 2×10^4, after the initial drop, E grows steadily and at $t = 1{\cdot}44$, it has attained a value of 20. The result confirms our experimental observation that transition occurs between 12500 and 17500.

Flow pattern

The perturbation streamlines for the case $R = 10^5$, $L = 2$, $\lambda = 0{\cdot}6$ at $t = 0{\cdot}15$ are shown in figure 5. Although this is not at the critical wavelength of 0·56, the flow pattern is not expected to differ much from the critical state. The streamlines exhibit pairs of counter-rotating vortices centred near the hot wall and displaced upward owing to the buoyancy effect. The flow pattern is entirely different from that obtained both in the physical and numerical experiments, which consists of a row of vortices of the same sign with strong shear at the boundaries. The present flow pattern is a necessary consequence of the assumption that all perturbation quantities are periodic in z as $\exp iKz$ (see also THS). It is physically plausible that the positive vortex is unstable since it flows against the buoyancy

generated near the hot wall. As a result the negative vortex would expand to fill almost the entire wavelength with the positive vortex squeezed into the strong shear region observed in experiments. This conjecture, however, awaits further analysis.

4. Conclusions

From the results obtained, the following conclusions may be drawn.

(i) It is immaterial what type of initial perturbation (whether in ω, T or S) is assumed. Consistent results can be obtained.

(ii) The effect of gap width on the rate of growth of perturbation kinetic energy and the critical wavelength is very small as long as the gap is larger than the characteristic length h.

(iii) The critical wavelength at $R = 10^5$ for $L = 1$ is $0{\cdot}54h$ and for $2 \leqslant L \leqslant 5$ is $0{\cdot}56h$. These values are comparable with the values $0{\cdot}65h$, obtained from the numerical experiment, and $0{\cdot}67$–$0{\cdot}97h$, obtained from the physical experiment.

(iv) The critical wavelength decreases slightly with increasing Rayleigh number.

(v) For a gap $L = 8$, the transition regime is determined to be between $R = 10^4$ and 2×10^4. Experimentally we have found the range to be 12 500–17 500.

(vi) The linear theory predicts a flow pattern consisting of counter-rotating vortices, which is not what has been observed in the experiments.

A substantial part of this work was performed when I was on research leave at DAMTP, University of Cambridge, during the academic year 1971–1972. The research leave was made possible by a Rutgers University Faculty Fellowship, for which I am grateful. I also wish to thank Professor G. K. Batchelor for providing me with a hospitable and stimulating environment in which to work. Part of this work was presented at the 13th International Conference of Theoretical and Applied Mechanics, Moscow, August 1972.

REFERENCES

CHEN, C. F., BRIGGS, D. G. & WIRTZ, R. A. 1971 Stability of thermal convection in a salinity gradient due to lateral heating. *Int. J. Heat & Mass Transfer*, **14**, 57–66.

CHEN, C. F. & KIRCHNER, R. P. 1971 Stability of time-dependent rotational Couette flow. Part 2. Stability analysis. *J. Fluid Mech.* **48**, 365–384.

CHEN, C. F., LIU, D. C. S. & SKOK, M. A. 1973 Stability of circular Couette flow with constant finite acceleration. *J. Appl. Mech.* **95**, 347–354.

FOSTER, T. D. 1965 Stability of homogeneous fluid cooled uniformly from above. *Phys. Fluids*, **8**, 1249–1257.

GRESHO, P. M. & SANI, R. L. 1971 The stability of fluid layer subjected to a step change in temperature: transient *vs.* frozen time analysis. *Int. J. Heat & Mass Transfer*, **14**, 207–222.

HART, J. E. 1971 On sideways diffusive instability. *J. Fluid Mech.* **49**, 279–288.

KELLER, H. B. 1968 *Numerical Methods for Two-point Boundary Value Problems*. Waltham, Mass.: Blaisdell.

Liu, D. C. S. & Chen, C. F. 1973 Numerical experiments on time-dependent rotational Couette flow. *J. Fluid Mech.* **59**, 77–98.

Mendenhall, C. E. & Mason, M. 1932 The stratified subsidence of fine particles. *Proc. U.S. Nat. Acad. Sci.* **9**, 199–207.

Thorpe, S. A., Hutt, P. K. & Soulsby, R. 1969 The effect of horizontal gradients on thermohaline convection. *J. Fluid Mech.* **38**, 375–400.

Wirtz, R. A. 1971 Physical and numerical experiments on cellular convection in a stratified fluid due to lateral heating. Ph.D. thesis, Rutgers University, New Brunswick, New Jersey.

Wirtz, R. A., Briggs, D. G. & Chen, C. F. 1972 Physical and numerical experiments on layered convection in a density-stratified fluid. *Geophys. Fluid Dyn.* **3**, 265–288.